Molecular Biology of the Cell
Vol. 16, 1200–1212, March 2005

Functional Analysis of Cytoplasmic Dynein Heavy Chain in *Caenorhabditis elegans* with Fast-acting Temperature-sensitive Mutations[D][V]

Diane J. Schmidt, Debra J. Rose, William M. Saxton, and Susan Strome

Department of Biology, Indiana University, Bloomington, IN 47405

Submitted June 26, 2004; Revised November 17, 2004; Accepted December 2, 2004
Monitoring Editor: Martin Chalfie

Cytoplasmic dynein, a minus-end–directed microtubule motor, has been implicated in many cellular and developmental processes. Identification of specific cellular processes that rely directly on dynein would be facilitated by a means to induce specific and rapid inhibition of its function. We have identified conditional variants of a *Caenorhabditis elegans* dynein heavy chain (DHC-1) that lose function within a minute of a modest temperature upshift. Mutant embryos generated at elevated temperature show defects in centrosome separation, pronuclear migration, rotation of the centrosome/nucleus complex, bipolar spindle assembly, anaphase chromosome segregation, and cytokinesis. Our analyses of mutant embryos generated at permissive temperature and then upshifted quickly just before events of interest indicate that DHC-1 is required specifically for rotation of the centrosome/nucleus complex, for chromosome congression to a well ordered metaphase plate, and for timely initiation of anaphase. Our results do not support the view that DHC-1 is required for anaphase B separation of spindle poles and chromosomes. A P-loop mutation identified in two independent dominant temperature-sensitive alleles of *dhc-1*, when engineered into the *DHC1* gene of *Saccharomyces cerevisiae*, conferred a dominant temperature-sensitive dynein loss-of-function phenotype. This suggests that temperature-sensitive mutations can be created for time-resolved function analyses of dyneins and perhaps other P-loop proteins in a variety of model systems.

INTRODUCTION

The active transport of proteins, RNAs, organelles, and chromosomes to specific destinations within cells is essential for normal development. In animal cells, two major classes of force-producing motor proteins, kinesins and dyneins, use the energy generated by ATP hydrolysis to drive the active transport of cargoes along microtubules, which act as directional tracks. Dyneins and kinesins with C-terminal motor domains move toward microtubule minus-ends, whereas kinesins with N-terminal motor domains move toward plus-ends (reviewed in Sawin and Scholey, 1991; Higuchi and Endow, 2002; Vale, 2003). The diverse forms of dyneins and kinesins and substantial experimental work have established that, despite the simplicity of bidirectional microtubule tracks, force generation and transport along them are complex. Specific processes require particular motors or sets of motors, and those motors are subject to precise regulatory controls. Although the full complement of microtubule motors has been identified in several model organisms, their functions and hence the mechanisms of many active transport processes remain poorly defined.

We focus here on questions about the functions of cytoplasmic dynein in mitosis and early patterning in *C. elegans* embryos. Cytoplasmic dynein is a multisubunit complex composed of two identical ~500-kDa heavy chains (DHCs) and several intermediate, light intermediate, and light chains (reviewed in Milisav, 1998; King, 2000; Vale, 2003). DHC is the force-producing component of the complex (Gibbons *et al*., 1991; Ogawa, 1991; Asai and Koonce, 2001). The globular DHC head encompasses six AAA domains, four of which contain a conserved nucleotide-binding P-loop motif (Gibbons *et al*., 1991; Ogawa, 1991; King, 2000). Projecting from the head is an intrachain coiled-coil stalk extension that mediates microtubule binding (Gee *et al*., 1997; Koonce, 1997). The N-terminal tail of DHC interacts with the intermediate, light intermediate, and light chains and with the $p150^{Glued}$ component of dynactin, a multisubunit, dynein-associated complex. These interacting proteins help regulate the activity, cargo specificity, and subcellular localization of dynein (reviewed in Milisav, 1998; Asai and Koonce, 2001; Vale, 2003).

Dynein is thought to participate in a variety of processes, including nuclear migration, centrosome separation, spindle formation, spindle alignment, chromosome segregation, nuclear envelope breakdown, mRNA localization, and organelle transport (Eshel *et al*., 1993; Li *et al*., 1993; Vaisberg *et al*., 1993; McGrail and Hays, 1997; Harada *et al*., 1998; Gönczy *et al*., 1999; Sharp *et al*., 2000a,b; Salina *et al*., 2002; Goshima and Vale, 2003). However, interpretation of the results of specific dynein inhibition experiments is complicated by the myriad of potential dynein functions. A failure of early dynein-dependent processes can have dramatic indirect effects on later processes of interest. Hence, a means to inactivate dynein function on a short timescale would be valuable.

We have determined that the *let-354* complementation group in *C. elegans* (Howell and Rose, 1990; Mains *et al*.,

This article was published online ahead of print in *MBC in Press* (http://www.molbiolcell.org/cgi/doi/10.1091/mbc.E04–06–0523) on December 22, 2004.

[D][V] The online version of this article contains supplemental material at *MBC Online* (http://www.molbiolcell.org).

Address correspondence to: Susan Strome (sstrome@bio.indiana.edu).

1990) corresponds to the *dhc-1* gene, which encodes a cytoplasmic dynein heavy chain, DHC-1 (Lye *et al*., 1987). Six alleles encode temperature-sensitive (ts) variants of DHC-1, and two of them have a missense mutation in a conserved P-loop residue. When we engineered it into the *DHC1* gene in budding yeast, that mutation caused a severe *dhc1* mutant phenotype that is ts. Using the *C. elegans dhc-1* ts alleles and a microscope stage whose temperature could be adjusted rapidly, we have addressed questions about specific dynein functions in early embryogenesis. By allowing mutant embryos to undergo early development at permissive temperature and then inactivating DHC-1 with a fast temperature shift just before an event of interest, we found evidence that dynein is required directly for rotation of the centrosome/nucleus complex onto the proper embryonic axis, for correct chromosome congression, and for timely initiation of anaphase. We did not find evidence that dynein is directly needed for anaphase spindle pole separation or for cytokinesis.

MATERIALS AND METHODS

Worm Strains

C. elegans strains were maintained as described by Brenner (1974). N2 variety Bristol was used as the wild-type strain. Other strains used in this study were as follows: KR1584 *let-354(h934) dpy-5(e61) unc-13(e450)/szT1[lon-2(e678) unc-29(e403)]* I; *+/szT1* X, and similar strains containing other *let-354* recessive alleles: *h72*, *h79*, *h90*, *h201*, *h267*, *h370*, *h390*, *h441*, *h482ts*, *h504*, *h508*, *h549*, *h693*, *h803*, *h809*, *h819*, *h841*, *h863*, *h866*; SS578 *let-354(h934) dpy-5(e61) unc-13(e450)/gaDp1* (I;f); BW503 *let-354(ct42ts)/unc-11(e47) dpy-5(e61)* I, and similar strains containing other *let-354* dominant ts alleles: *ct76ts*, *ct77ts*, and *sb42ts*; EU654 *dhc-1(or195ts)* I; AZ212 *unc-119(ed3)*; *ruIs32*[*unc119(+) pie-1::gfp::histone H2B*] III; WH204 *unc-119(ed3)*; *ojIs1*[*unc119(+) pie-1::gfp::tbb-2*]; TH32 *unc-119(ed3)*; *ruIs32*[*unc119(+) pie-1::gfp::histone H2B*] III; *ddls6* [*unc119(+) pie-1::gfp::tbg-1*]; SS645 *let-354(ct76ts)/unc-11(e47) dpy-5(e61)* I; *ruIs32*[*unc119(+) pie-1::gfp::histone H2B*] III; SS651 *let-354(ct76ts)/unc-11(e47) dpy-5(e61)* I; *ojIs1*[*unc119(+) pie-1::gfp::tbb-2*]; SS824 *dhc-1(or195ts)* I; *ruIs32*[*unc119(+) pie-1::gfp::histone H2B*] III; *ddls6* [*unc119(+) pie-1::gfp::tbg-1*]; and KR1737 *hDf6 dpy-5(e61) unc-13(e450)*I; *hDp31*(I;f).

Strains were kindly provided by Paul Mains (University of Calgary, Calgary, Alberta, Canada), Ann Rose (University of British Columbia, Vancouver, British Columbia, Canada), D. Hamill (Ohio Wesleyan University, Delaware, OH), B. Bowerman (University of Oregon, Eugene, OR), J. White (University of Wisconsin, Madison, WI), A. Hyman (Max Planck Institute of Molecular Cell Biology and Genetics, Dresden, Germany), A. Desai (University of California, San Diego, San Diego, CA), and the *Caenorhabditis* Genetics Center (University of Minnesota, Minneapolis, MN).

Transformation Rescue

let-354(h934) dpy-5 unc-13/gaDp1 adult hermaphrodites were injected with a mixture of 2 ng/μl cosmid T21E12 DNA (linearized with *Sac*II), 2 ng/μl cosmid ZK973 DNA (linearized with *Not*I), and 100 ng/μl pRF4 *rol-6(su1006)* DNA (linearized with *Sma*I). Cosmid DNA was prepared using the QIAGEN (Valencia, CA) maxiprep protocol, and plasmid DNA was prepared using the QIAGEN miniprep protocol. Two independent F1 lines of rescued *let-354(h934) dpy-5 unc-13* worms were obtained. Those lines were Dpy Unc, which obscured the Rol-6 phenotype caused by the presence of a *rol-6(su1006)*-bearing extrachromosomal array, so the presence of an array was confirmed in two ways. Mating of rescued Dpy Unc hermaphrodites to N2 males resulted in the production of some Rol-6 outcross progeny. Rescued Dpy Unc hermaphrodites fixed and stained with Hoechst 33342 contained in their oocytes six bivalents and an extrachromosomal DNA mass.

Sequencing

Genomic DNA was extracted from *let-354/unc-11 dpy-5* heterozygous hermaphrodites bearing each of three dominant ts alleles of *let-354* (*ct42*, *ct76*, and *ct77*) by using a standard phenol/chloroform extraction method (Maniatis *et al*., 1982) followed by column purification using QIAGEN Genomic 100/G columns. DNA segments spanning the predicted coding region (~15 kb) of *dhc-1* were polymerase chain reaction (PCR) amplified and sequenced by SeqWright DNA Sequencing (Houston, TX). We confirmed mutant changes by targeted sequencing of specific portions of PCR-amplified *dhc-1* DNA from five to 10 heterozygous worms and from five to 10 N2 worms, by using an ABI 3700 prism automated fluorescent sequencer (Indiana University Molecular Biology Institute, Bloomington, IN).

Yeast Transformation

Yeast strains YEF473a and YEF473a *dhc1*Δ::HIS3 and plasmid CYDHC/GEM containing the full-length yeast dynein heavy chain gene *DHC1* (a gift from K. Bloom, University of North Carolina, Chapel Hill, NC) were used to test whether the P-loop mutation found in *let-354(ct77)* and (*ct42*) would cause a dominant ts *dhc1* mutant phenotype in yeast. The mutation was engineered into the yeast *DHC1* gene by using PCR-based site-directed mutagenesis. A 1-kb fragment containing the third P-loop of *DHC1* was cut from CYDHC/GEM, PCR amplified using primers 5′ GCG AAG AGT TCC GGA GTG CAT TAT TCA TAA TCA TTG TTT TAC CAG ATT CAG GTG GCC CAC AAA GG 3′ and 5′ ATA TGG TGG GTG CTT CTT CG 3′, and reintroduced back into the CYDHC/GEM plasmid to generate CYDHC*/GEM. To allow expression in yeast, the CYDHC* insert was transferred into pRS316 plasmid (a gift from A. Bender, Indiana University) and introduced into yeast by using either electroporation (protocol adapted from D. Gottschling, Fred Hutchinson Cancer Research Center, Seattle, WA; http://iprotocol.mit.edu/protocol/100.htm) or lithium acetate (Walhout and Vidal, 2001). Transformed yeast were selectively grown on URA$^-$ plates, and then grown for 1–4 h at 16 or 30°C in YPD medium (BD Biosciences Clontech, Palo Alto, CA). Cells were fixed by standard methanol/acetone fixation, stained with 4,6-diamidino-2-phenylindole (DAPI), and scored for one nucleus or two or more nuclei on a Zeiss (Carl Zeiss, Thornwood, NY) Axioskop by using differential interference contrast (DIC) and fluorescence microscopy. To confirm the sequence change, plasmid was isolated from transformed yeast and the relevant region was sequenced.

Analysis of Embryonic Development by Time-Lapse DIC and Confocal Fluorescence Microscopy

Embryos were mounted in M9 buffer (Brenner, 1974) on 2% agarose pads containing a fine-Teflon PTFE-insulated probe connected to a Cole-Parmer Instrument (Vernon Hills, IL) Digisense thermocouple thermometer to monitor temperature and covered with a coverslip. DIC images were obtained on a Zeiss Axioplan microscope with a Hamamatsu C2400 camera and video controller with an Argus-10 image processor (Hamamatsu City, Japan). Images were captured every 3 s by using NIH Image (version 1.62b7, developed by Wayne Rasband, National Institutes of Health, Bethesda, MD and available at http://rsb.info.nih.gov/nih-image). Fluorescence images were obtained on a Nikon Optiphot microscope with a Bio-Rad MRC600 scanning confocal system (Hercules, CA) and collected as a time series by using MRC600 software. Images were captured every 6 s for green fluorescent protein (GFP)::histone time-lapse movies or every 10 s for GFP::tubulin time-lapse movies. Stacks of images were manipulated to generate figures in NIH Image.

Rapid temperature-upshift experiments were performed using a temperature-control microscope stage (Supplemental Figure s1) in a microscope room held at 16°C. Embryos were prepared and mounted on slides with agar pads at 16°C, placed on the microscope stage, observed, and shifted to 25°C just before an event of interest. Based on the read-out from a thermocouple probe mounted in the agar pad immediately adjacent to embryos, a shift from 16 to 25°C took 24–40 s.

Antibodies and Immunofluorescence Microscopy

To generate antisera against *C. elegans* DHC-1, a 17-amino acid peptide, MDSGNESSIIQPPNLKC, corresponding to the N-terminal 16 amino acids plus an additional cysteine, was synthesized and conjugated to maleimide-activated keyhole limpet hemocyanin (Research Genetics, Huntsville, AL). The peptide was used to immunize rabbits (Cocalico Biologicals, Reamstown, PA). Affinity-purified antibodies were prepared by passage over a column of DHC-1 peptide coupled to Sulfolink coupling gel (Pierce Chemical, Rockford, IL). Bound antibodies were eluted with 100 mM glycine, pH 2.5, dialyzed against phosphate-buffered saline, and concentrated (5-fold). Figure 1 demonstrates that the antibody is specific for DHC-1.

For immunofluorescent staining of embryos, adult hermaphrodites were cut, fixed, and stained as described previously (Strome and Wood, 1983). The primary antibodies used were anti-DHC-1 at 1:200, anti-DNC-1 at 1:200 (a gift from H. Zhang and J. White, University of Wisconsin), and mouse 4A1 anti-α-tubulin at 1:50 (a gift from M. Fuller, Stanford University School of Medicine, Stanford, CA; Piperno and Fuller, 1985). The secondary antibodies used were Alexa488 goat anti-mouse and Alexa594 goat anti-rabbit (Molecular Probes, Eugene, OR). Embryos were counterstained with DAPI to visualize DNA. Anti-DHC-1 and anti-tubulin images were collected as Z-series of 1.0-μm slices on a Bio-Rad MRC600 microscope, or on a PerkinElmer Ultraview LCI30E spinning disk confocal microscope by using Ultraview software (PerkinElmer Life and Analytical Sciences, Boston, MA). DNA images were collected with a Hamamatsu ORCA-ER digital camera on a Nikon (Tokyo, Japan) Eclipse E800 microscope with MetaMorph (Universal Imaging, Downingtown, PA) software. Images were processed using Photoshop 7.0 (Adobe Systems, Palo Alto, CA).

RNA Interference (RNAi)

dhc-1 cDNA clones yk27b2 and yk35d8 were obtained from Y. Kohara (National Institute of Genetics, Mishima, Japan). Phagemid DNA and double-

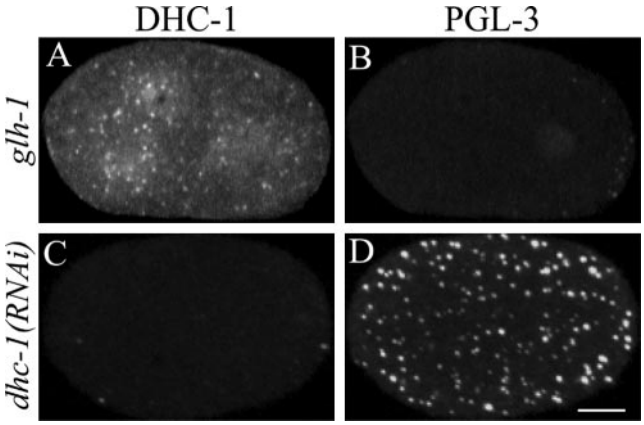

Figure 1. Test of anti-DHC-1 antibody specificity. Rabbit antibodies were raised against the amino terminal 16 amino acids of DHC-1, affinity purified, and used to stain *dhc-1(+) glh-1(gk100)* embryos and *dhc-1(RNAi)* embryos. Both types of embryos were dissected, fixed, and stained together on the same slide to ensure identical treatment. *glh-1* mutant embryos lack detectable staining by rat anti-PGL-3 (a marker for P granules) (Meyer and Strome, unpublished data), allowing control *dhc-1(+) glh-1* embryos to be distinguished from *dhc-1(RNAi)* embryos. (A and B) Control 2-cell embryo containing DHC-1 (A) and lacking PGL-3 (B). (C and D) Nearby 1-cell RNAi embryo lacking detectable DHC-1 (C) and containing PGL-3 (D). Images are projections of Z-series from a spinning disk confocal fluorescence microscope. Embryos in this and subsequent figures are oriented with posterior to the right. Bar, 10 μm.

stranded RNA (dsRNA) for injection were prepared as described previously (Strome *et al*., 2001). dsRNA at a concentration of 1 mg/ml was injected into young adult hermaphrodites. Embryos produced by injected parents were analyzed 18–24 h postinjection. A *dhc-1* dsRNA feeding construct was engineered by transferring a 3.1-kb *dhc-1* cDNA fragment into plasmid L4440 and transforming HT115(DE3) bacterial cells (Invitrogen, Carlsbad, CA). The dsRNA-expressing bacteria were grown using the protocol of Kamath *et al*. (2000).

RESULTS

Temperature-sensitive Alleles of C. elegans dhc-1

To pursue studies of cytoplasmic dynein in early *C. elegans* embryos, we sought genetic mutations that would inhibit the function of its force-producing subunit, DHC-1. Two findings suggested that the *let-354* complementation group represents alleles of the *dhc-1* gene: 1) *let-354* maps genetically to a region of chromosome I that contains *dhc-1* (Howell and Rose, 1990; Mains *et al*., 1990; The *C. elegans* Sequencing Consortium, 1998), and 2) RNAi depletion of DHC-1 causes developmental defects similar to those seen in *let-354* mutants (see below; Mains *et al*., 1990; Gönzcy *et al*., 1999). To determine whether the *let-354* complementation group indeed corresponds to the *dhc-1* gene, we first tested whether *dhc-1* genomic DNA could rescue the larval lethal mutant phenotype of *let-354* recessive alleles. Cotransformation of *let-354(h934)/+* hermaphrodites with two overlapping cosmids (T21E12 and ZK973), which together encompass the *dhc-1* coding sequence, as well as 13 other predicted genes, generated extrachromosomal transgenic arrays that rescued the lethality of *let-354(h934)/let-354(h934)* mutant progeny.

To determine whether *let-354* mutations affect the expression or distribution of DHC-1, we compared DHC-1 staining in wild-type and mutant embryos (Figure 2), focusing on the dominant ts *let-354* alleles isolated by Paul Mains (*ct42*, *ct76*, *ct77*, and *sb42*) (Mains *et al*., 1990). Animals homozygous for those alleles are not viable at any temperature. Heterozygotes are viable at 16°C and maternal-effect lethal at 25°C (see below). Affinity-purified antibodies revealed a distribution of DHC-1 in wild-type embryos similar to that described previously (Gönczy *et al*., 1999): punctate in cytoplasm, an elevated concentration on nuclear envelopes during pronuclear migration, enrichment in the central spindle during metaphase, and faint enrichment over the entire anaphase spindle (Figure 2, A–C). We also noted a transient accumulation of DHC-1 in a narrow cortical zone between the AB and P_1 cells during rotation of the P_1 centrosome-centrosome axis onto the anterior-posterior (AP) axis (Figure 2D). This supports the hypothesis that cortically anchored dynein in that cortical zone pulls on astral microtubules to generate force for the rotation (Skop and White, 1998).

Embryos derived from mothers heterozygous for any of the dominant ts alleles of *let-354* that had been cultured at 25°C for 24 h showed abnormally heavy concentrations of DHC-1 at prophase centrosomes and mitotic spindle poles (Figure 2, E–G). A recessive ts *dhc-1* allele, *or195* (Hamill *et al*., 2002), caused a similar accumulation of DHC-1 on centrosomes at 25°C (Figure 2H). Interestingly, DHC-1 concentration on centrosomes also was seen at permissive temperature (16°C) with both dominant and recessive ts alleles (Supplemental Figure s2, E and F). To determine whether the accumulation reflected aberrant behavior of the entire dynein–dynactin complex, we tested the effects of *let-354* ts alleles on the distribution of DNC-1, the dynactin $p150^{Glued}$ ortholog in worms. It, too, concentrated heavily at centrosomes (Supplemental Figure s2, C and D). These observations, showing that both recessive and dominant ts *let-354* alleles cause the dynein–dynactin complex to mislocalize, are consistent with the identity of *let-354* as *dhc-1*.

To search for specific *let-354* ts mutant changes, we sequenced the *dhc-1* coding regions of three dominant ts strains (Figure 3). In *ct76*, a conserved alanine in the Box VI motif of the fourth AAA domain is changed to an aspartic acid. In *ct42* and *ct77*, the same G→A base change replaces glycine2540 in the third P-loop with glutamic acid. P-loops, with a consensus of GxxgxGKT/S (where x is anything and g is common), are key features of ATP-binding sites in dynein heavy chains and a variety of other NTPases, including myosins, kinesins, ATP synthase, and Ras (Walker *et al*., 1982; Gibbons *et al*., 1991; Shen *et al*., 1994; Kull *et al*., 1996; Deyrup *et al*., 1998). Glycine2540 corresponds to "g" at position 4 in the P-loop consensus. These results confirmed that the *let-354* complementation group corresponds to the *dhc-1* gene and raised the possibility that dynein heavy chains in other organisms might be rendered temperature sensitive by equivalent mutations.

An Engineered Dominant Temperature-sensitive DHC1 in Budding Yeast

To determine whether the *ct42-ct77* P-loop mutation has a dominant ts effect on dynein in other species, the equivalent G-to-E codon change was tested in the *DHC1* gene of *Saccharomyces cerevisiae*. A deletion-disruption mutation of *DHC1* (*dhc1*Δ) impairs translocation of the daughter nucleus to the bud-cell at the end of mitosis. It is not lethal but causes a significant percentage of mutant cells to carry two or more nuclei (Eshel *et al*., 1993; Li *et al*., 1993). Yeast cells were transformed with either a mutant *dhc1(G-E)* gene or a wild-type *DHC1* gene in a low copy number plasmid. The effects of each on dynein function were tested in wild-type and *dhc1*Δ backgrounds by counting multinucleate cells after growth at 16 or 30°C (Table 1; statistical analysis is in Sup-

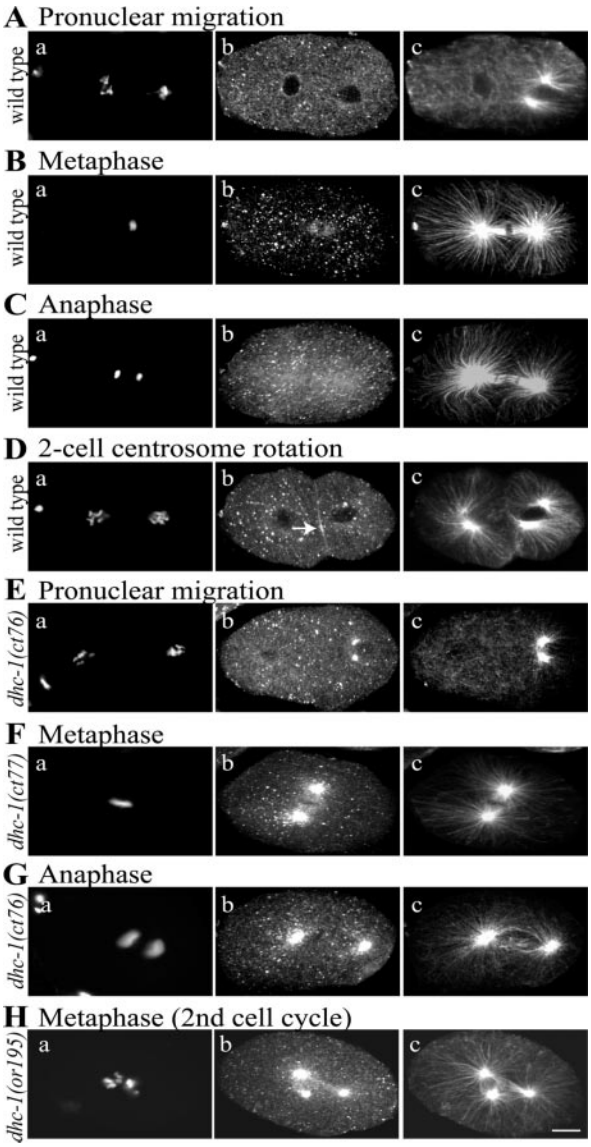

Figure 2. DHC-1 distribution in wild-type and *dhc-1* embryos. Fixed embryos were stained with DAPI (a), affinity-purified rabbit anti-DHC-1 (b), and mouse anti-tubulin (c). Images in panels a are from a widefield fluorescence microscope. Images in b and c are projections of Z-series from a scanning confocal fluorescence microscope. All embryos displayed punctate DHC-1 staining in the cytoplasm; other localized concentrations are described below. (A–D) Wild-type embryos. (A) DHC-1 is lightly concentrated around the oocyte pronuclear envelope during pronuclear migration. (B) DHC-1 is lightly concentrated on the central spindle at metaphase; there is no concentration on spindle poles. (C) DHC-1 is faintly concentrated on the anaphase spindle and spindle poles. (D) During rotation of the P_1 cell centrosome/nucleus complex (on the right), DHC-1 is concentrated at the cell periphery between AB and P_1 in the region (arrow) toward which one centrosome (the lower one in c) is moving. (E–H) *dhc-1* one-cell embryos from *ct76/+*, *ct77/+*, or *or195* hermaphrodites shifted to 25°C for 24 h. At all stages, DHC-1 shows the normal distribution and in addition a dramatic accumulation on the microtubule organizing centers, initially the centrosomes associated with the sperm pronucleus (E) and later the poles of the mitotic spindle (F–H). Mutant embryos like that shown in H are multipolar due to continued centrosome replication after a failed first cleavage. The *dhc-1* embryos shown in this figure contain uncharacteristically well-formed spindles, to highlight the concentration of DHC-1 on spindle poles. Similar pole concentrations also were observed in mutant embryos with small or monopolar spindles. Bar, 10 μm.

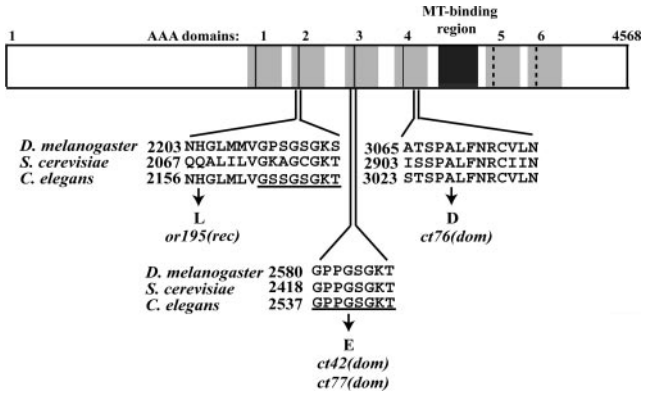

Figure 3. Amino acid changes caused by ts mutations in the *dhc-1* gene. The six AAA domains are shown as gray boxes. The first four AAA domains have conserved P-loops (black lines), whereas the fifth and sixth AAA domains have diverged P-loops (dashed black lines). The coiled-coil, microtubule-binding stalk region is shown as a black box. The dominant ts *dhc-1* allele *ct76* contains a mutation (G→A) that causes an A3027D replacement in the Box VI element within AAA4. Two other dominant ts *dhc-1* alleles, *ct42* and *ct77*, both contain the same base pair substitution (G→A), which results in a G2540E change in the third P-loop (underlined). The recessive ts *dhc-1* allele *or195* has a mutation that causes an H2157L replacement near the second P-loop (underlined; Hamill *et al*., 2002). Accession numbers: *Drosophila*, P37276; *S. cerevisiae*, P36022; and *C. elegans*, NP491363.

plemental Table s1). At both temperatures, the wild-type transgene had little effect on wild-type cells and substantially reduced the multinucleate phenotype of *dhc1*Δ cells. In contrast, the *dhc1(G-E)* transgene in the wild-type background at 30°C caused multinucleate cells at a frequency equivalent to that observed in *dhc1*Δ (~17%). That effect was significantly reduced at 16°C but was not eliminated (3.2%). Interestingly, in the *dhc1*Δ background at 30°C, the *dhc1(G-E)* transgene caused a modest but significant increase in the percentage of multinucleate cells (23%) relative to that observed with *dhc1*Δ alone (17%), suggesting that the mutant motor has a slightly inhibitory effect on the dynein-independent mechanism for nuclear migration. These results demonstrate that the *C. elegans dhc-1(ct42-ct77)* G-E change, when placed in DHC of an evolutionarily distant organism, causes a dominant ts phenotype. This confirms in vivo that the third P-loop is essential for proper dynein function (Silvanovich *et al*., 2003; Reck-Peterson and Vale, 2004) and highlights the possibility that equivalent mutations can be used to create dominant ts versions of a variety of other P-loop proteins.

Processes Influenced by Inhibition of DHC-1

To assess which events in early embryogenesis are impaired by *dhc-1* mutations, we compared wild-type, *dhc-1(RNAi)*, and *dhc-1* ts mutant embryos by time-lapse DIC microscopy (Figure 4, Videos 1–6, and Table 2). The progression of events in wild-type is illustrated in Figure 4A and in Video 1 (supplemental data). As described previously by Gönczy *et al*. (1999), RNAi depletion of DHC-1 from the maternal germline results in severe defects in 1-cell embryos (Figure 4B, Video 2, and Table 2). In embryos produced 24 h after dsRNA injection, the sperm pronucleus did not leave the posterior cortex, the oocyte pronucleus did not show a fast phase of migration, and hence pronuclei failed to meet before nuclear envelope breakdown (NEB) (Figure 4B, a–d). A

Table 1. Dominant ts effect of a G→E change in the third P-loop of yeast DHC-1

Yeast strain	Plasmid	Temp. (°C)	% Cells with >1 nucleus[a]	n[b]
Wild type		30	0.2	403
		16	0	298
Wild type	*dhc1*(G→E)[c]	30	17.4	339
		16	3.2	219
Wild type	*DHC1*[d]	30	0	328
		16	0.8	380
*dhc1*Δ		30	17.3	347
		16	28.2	298
*dhc1*Δ	*dhc1*(G→E)[c]	30	23.2	387
		16	31.2	269
*dhc1*Δ	*DHC1*[d]	30	2.1	334
		16	4.0	373

Transformed or untransformed haploid cells were grown for 2–4 h in YPD medium after selection on URA$^-$ plates. Statistical analysis of the data is in Supplemental Table s1.

[a] Yeast cells were fixed and stained with DAPI. Dividing cells (i.e. cells with buds) were scored for the presence of more than one nucleus.

[b] Total number of dividing cells.

[c] Plasmid containing full-length *dhc1* with a mutation that causes Gly2421 to be replaced by Glu.

[d] Plasmid containing full-length wild-type DHC-1.

bipolar spindle was not evident, and cytokinesis did not occur. Instead, RNAi embryos underwent dramatic cortical blebbing, and multiple nuclei formed in the posterior cytoplasm during telophase (Figure 4B, f and g). By 36 h after RNA injection, existing oocytes were aberrant and the gonad stopped producing new oocytes. This indicates that DHC-1 serves essential roles in the maternal germline and raises the possibility that defects in germline physiology contribute nonspecifically to the phenotypes observed in *dhc-1(RNAi)* embryos.

Our analysis of events in *dhc-1* mutant embryos was performed with six ts alleles: the dominant *ct42*, *ct76*, *ct77*, and *sb42*, plus the recessive *or195* and *h482* (Howell and Rose, 1990; Mains *et al*., 1990; Mitenko *et al*., 1997; Hamill *et al*., 2002). The 19 nonconditional recessive alleles result in larval lethality: homozygous progeny from heterozygous mothers undergo apparently normal embryo development, hatch, and arrest at a midlarval stage (Howell and Rose 1990). The different ts alleles of *dhc-1* create different pools of DHC-1 dimer. Early embryos from mothers homozygous for a recessive ts allele contain fully mutant dimers, whereas early embryos from mothers heterozygous for a dominant ts allele are presumed to contain a mix of fully mutant dimers, fully wild-type dimers, and heterodimers with one mutant and one wild-type subunit. To simplify wording below, embryos derived from both types of mothers will be referred to as *dhc-1* ts mutant embryos. *dhc-1* ts embryos displayed low levels of embryonic lethality at permissive temperature (16°C) and 100% lethality at elevated temperature: 18.4°C in *ct76* and 20°C in *ct77-ct42* (Supplemental Table s2).

Our initial studies of the conditional mutants involved shifting mutant mothers (as L4 larvae) to a restrictive temperature (25°C) for 24 h and then analyzing their early embryos by time-lapse DIC microscopy at 25°C. The embryonic processes affected by this temperature regime were similar for all the ts alleles, but the severities of defects varied, indicating an allelic series as follows: strongest—*ct76*, *or195*, *ct77-ct42*, *sb42*, *h482*—weakest. To test the severity of a strong allele over a null, we examined embryos from worms carrying the recessive allele *or195* over a deficiency of the region, *hDf6* (Table 2). The phenotypes of embryos from *dhc-1(or195)/hDf6* mutants at 25°C were slightly more severe than those of *dhc-1(or195)/dhc-1(or195)* and similar to those of *dhc-1(ct76)*. This suggests that although neither *or195* nor *ct76* is a null allele, they do cause a nearly complete loss of function. We saw no evidence of a neomorphic gain of function here or in other tests.

Pronuclear Migration. Although *dhc-1* ts mutant embryos at 25°C showed some defects in meiosis (our unpublished data), normal pronuclei usually formed (Figure 4, D and E, and Videos 4 and 5). In *ct76* embryos (Figure 4D and Video 4), the female pronucleus seemed to migrate slowly and met the advancing male pronucleus near the midpoint of the embryo rather than in the posterior half (Figure 4D, b). To quantify this effect, the position of the center of the female pronucleus was measured as a function of time. In wild-type embryos (n = 10), an initial "slow phase" of migration (0.035 ± 0.004 μm/s) moved the female pronucleus to ~37% of embryo length (EL; anterior pole is 0%, posterior pole is 100%); a subsequent "fast phase" (0.26 ± 0.03 μm/s) moved it to the sperm pronucleus at 69 ± 4% EL. In *ct76* embryos (n = 10), the slow phase was normal (0.035 ± 0.004 μm/s), but the fast phase was only 0.13 ± 0.07 μm/s and the pronuclei met at 58 ± 3% EL. Thus, the *ct76* lesion reduces but does not eliminate the fast phase of migration. Other *dhc-1* ts alleles also affect pronuclear migration, causing the pronuclei to meet more centrally than in wild type (Supplemental Table s3)

Centrosome Movements and Spindle Formation. It was evident that restrictive temperature also affected the behavior of centrosomes in *dhc-1* ts mutant embryos. In wild type (Figure 4A and Video 1), newly duplicated centrosomes on the male pronucleus move away from one another, separating to opposite sides, usually producing a centrosome-centrosome axis that lies transverse to the AP axis of the embryo. As male and female pronuclei meet, the centrosome/nucleus complex rotates 90° to align the centrosomes on the AP axis (Figure 4A, b–d). In embryos from *dhc-1* ts mutant mothers cultured at permissive temperature, these processes looked normal (e.g., Figure 4C and Video 3). Of 16 *dhc-1(ct76)* embryos grown at restrictive temperature, centrosome separation failed completely in five, leading to forma-

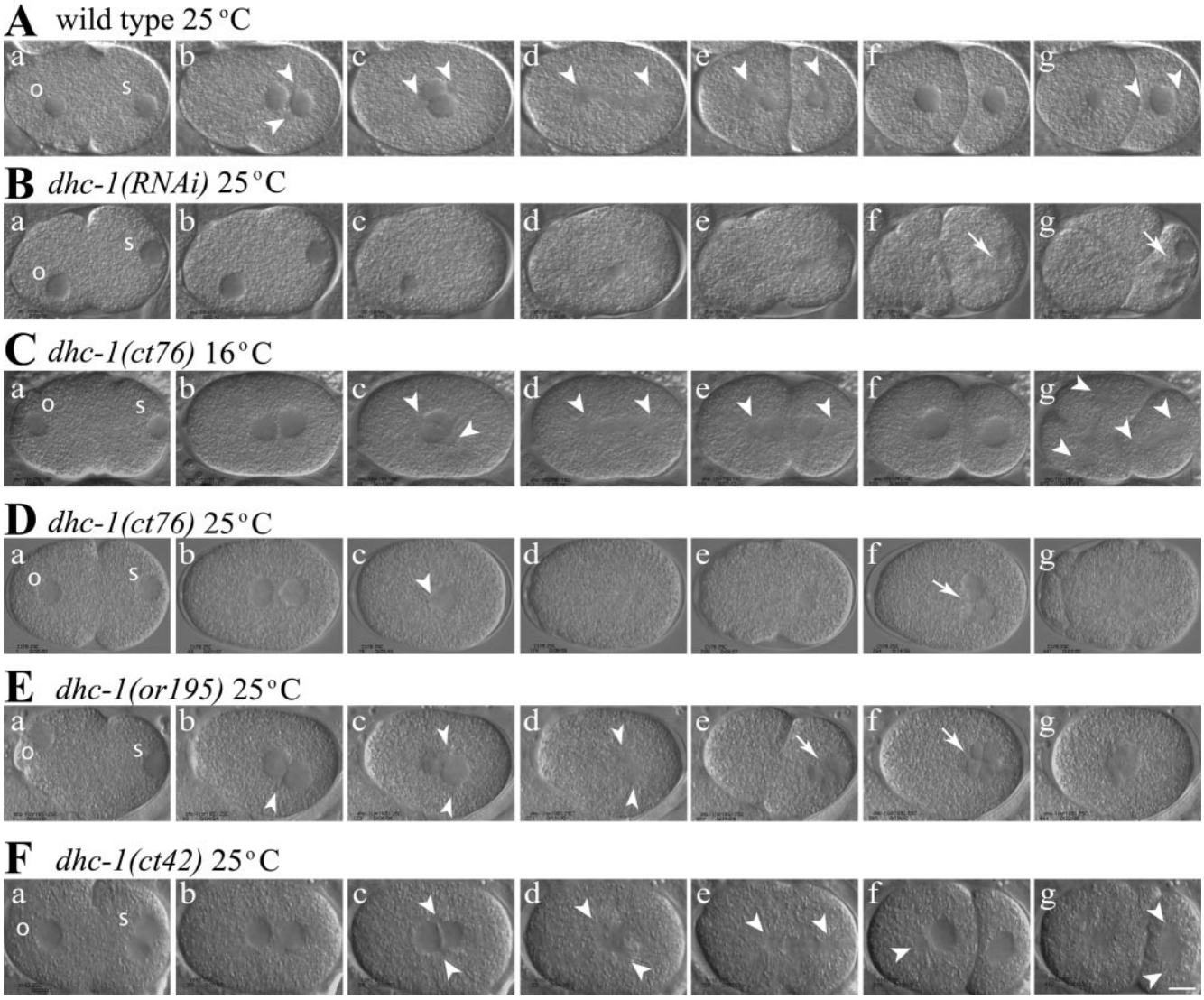

Figure 4. Early development of wild-type, *dhc-1(RNAi)*, and *dhc-1* mutant embryos. Each image is a single frame from a time-lapse movie of a live embryo captured using DIC microscopy. Arrowheads indicate centrosomes, and arrows point to micronuclei. Oocyte pronuclei are marked with "o" and sperm pronuclei with "s" in the first frame of each series. In all cases (except C), embryos were dissected from hermaphrodites 24 h after a shift from 16 to 25°C, initiated when the mothers were L4 larvae. (A and Video 1) Wild-type embryo. (A, a and b) Pronuclear migration and meeting. (A, c) Rotation of the centrosome/nucleus complex. (A, d) Anaphase with a shift of the posterior spindle pole toward the posterior cortex. (A, e) Posterior spindle pole flattening. (A, g) P_1 centrosome axis alignment with the AP axis. (B and Video 2) *dhc-1(RNAi)* embryo. (B, a–c) Pronuclei failed to migrate. (B, d and e) Bipolar spindle assembly failed. (B, f and g) Chromosome separation failure produced multiple micronuclei. (B, e–g) Cytokinesis failed, although numerous transient membrane invaginations formed. (C and Video 3) Embryo from a *dhc-1(ct76)*/+ hermaphrodite raised at permissive temperature (16°C). All events resembled wild type, except that the posterior spindle pole did not flatten (C, e). (D and Video 4) Embryo from a *dhc-1(ct76)*/+ hermaphrodite. (D, a and b) Pronuclei met more centrally than in wild type. (D, c–e) Centrosome separation failed, and a bipolar spindle failed to form. (D, d and e) Posterior shift of the monopolar spindle. (D, f and g) Chromosome separation and cytokinesis failed. (E and Video 5) Embryo from a *dhc-1(or195)* hermaphrodite. (E, a and b) A minority case in which pronuclei met at a normal posterior position. (E, b–d) Centrosomes separated, but the centrosome axis failed to rotate and a stunted spindle formed on the transverse axis. (E, d and e) Posterior shift of the spindle. (E, e–g) Chromosome separation and cytokinesis failed. (F and Video 6) Embryo from a *dhc-1(ct42)*/+ hermaphrodite. (F, a) Occasionally two sperm pronuclei were observed in mutant embryos. (F, b) The pronuclei met near the center. (F, c and d) Centrosomes separated, but the centrosome axis did not rotate fully onto the AP axis. (F, d–f) A small spindle formed and moved toward the posterior cortex, chromosomes separated, and cytokinesis occurred. (F, g) The centrosome axis failed to rotate in P_1, and cytokinesis failed in AB. Bar, 10 μm.

tion of a monopolar first spindle (Figures 4D, b–d, and 5A). In the remaining 11 embryos, centrosome separation was delayed until after the pronuclei met. In some cases, delayed separation was transverse to the AP axis, and in other cases it was along the AP axis. Rotation of the centrosome/nucleus complex failed or was partial in most embryos with transversely separated centrosomes (Table 2). In all cases with full separation, centrosomes collapsed toward one another after NEB, and abnormally small spindles formed. In *or195*, *ct77*, and *ct42* embryos, initial centrosome separation was successful, centrosomes usually collapsed toward one another after NEB, and small spindles formed. Rotation onto

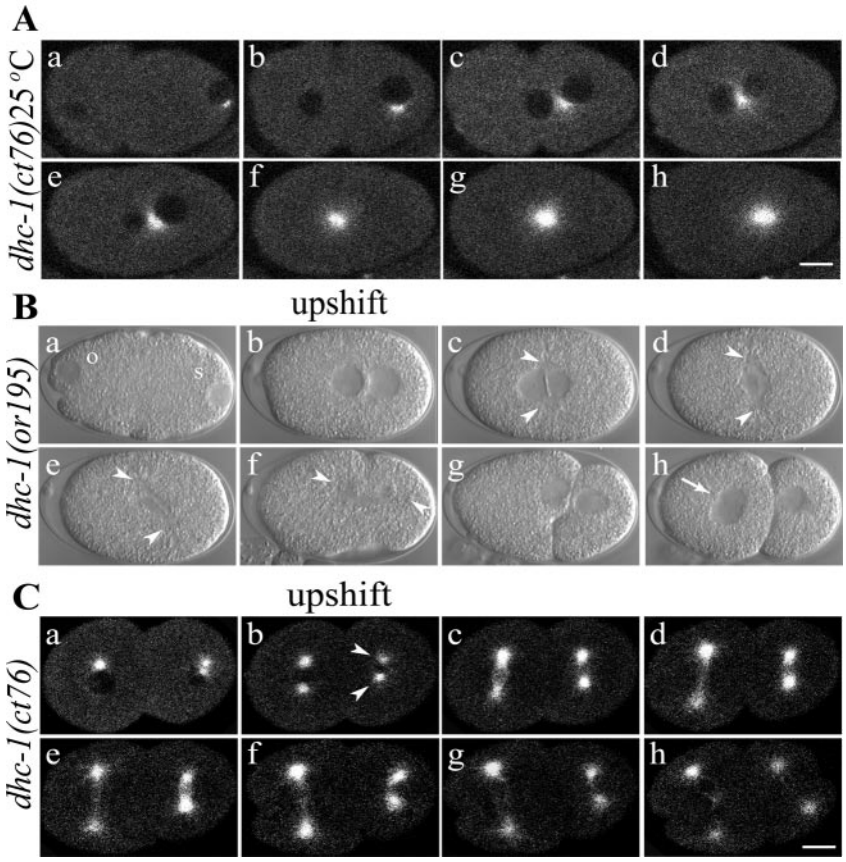

Figure 5. Rotation of centrosomes fails in *dhc-1* ts mutant embryos upshifted just before the rotation period. (A) Time-lapse confocal fluorescence images of an embryo from a *dhc-1(ct76)/+* hermaphrodite expressing GFP::β-tubulin. Embryos generated at 25°C (Figure 4D) or shifted to 25°C early, in this case at the beginning of pronuclear migration (a), fail in centrosome separation (b–h). (B and Video 8) Time-lapse DIC microscopy images of a *dhc-1(or195)* embryo upshifted from 16 to 25°C after centrosome separation and pronuclear migration (b). The centrosome/nucleus complex failed to rotate from the transverse onto the AP axis, and after NEB the mitotic spindle formed transverse to the AP axis (c and d, arrowheads point to centrosomes in c and spindle poles in d) (see Figure 4, A and C, for normal rotation). Subsequent movement of one spindle pole toward the posterior cortex during anaphase eventually resulted in spindle orientation and position that resembled wild type (e and f). Chromosome segregation and cytokinesis occurred but were defective, as evidenced by the aberrant cleavage furrow (g) and the double nucleus in AB (h, arrow). (C and Video 9) Time-lapse confocal images of a two-cell embryo from a *dhc-1(ct76)/+*; GFP::β-tubulin hermaphrodite. The embryo was upshifted after the centrosomes in P_1 (b, arrowheads) had begun to separate. The centrosome/nucleus complex failed to rotate (c and d), and a mitotic spindle formed transverse to the AP axis (d–g). Bar, 10 μm.

the AP axis was often defective (Figure 4E, d and F, d; Videos 5 and 6; and Table 2), especially in *or195*, which is the strongest of the three alleles. Overall, our analysis of *dhc-1* ts mutant and RNAi embryos as well as the RNAi studies of Gönczy *et al*. (1999) agree that loss of cytoplasmic DHC function inhibits centrosome separation, causes separated centrosomes to collapse toward one another after NEB, and inhibits rotation of the centrosome axis into alignment with the AP axis.

Anaphase. Time-lapse DIC movies revealed that anaphase chromosome separation failed in the most severe *dhc-1* ts mutants (Figure 4, D and E, and Table 2). In wild type (Figure 4A and Video 1), anaphase consists of spindle elongation (anaphase B) with no chromosome-to-pole movement (anaphase A) (Oegema *et al*., 2001). The anterior pole moves little, whereas the posterior pole moves toward the posterior cortex and oscillates dramatically from side to side, rocking the spindle. The posterior centrosome subsequently flattens, whereas the anterior centrosome remains spherical. In embryos from *dhc-1* ts mutant mothers held at permissive temperature, these processes looked normal, except that posterior centrosome rocking and flattening did not occur in the five strongest ts alleles (Videos 3 and 7; our unpublished data). At restrictive temperature in severe ts mutants (*ct76* and *or195*), stunted bipolar spindles rarely elongated and chromosomes did not separate (Figure 4, D and E; Videos 4 and 5; and Table 2). Notably however, during anaphase the monopolar or small bipolar spindles did migrate toward the posterior cortex, leading to formation of micronuclei in the posterior hemisphere. Subsequently, a cleavage furrow usually formed, but cytokinesis was not successful. Subsequent cell cycles continued and aberrant mitosis/cytokinesis resulted in multinucleate, sometimes multicellular, embryos. The less severe ts mutants often completed the first division cycle successfully and then failed in later cycles (Figure 4F, Video 6, and Table 2).

To investigate whether DHC-1 contributes to the posterior spindle shift that ensures an asymmetric P_0 division in normal embryos, we measured changes in the position of the posterior centrosome as a function of time (Supplemental Table s3). After pronuclei met and moved to the center of the embryo, the position of the point of contact between the two pronuclei (the approximate position of both centrosomes) was not distinguishable in wild-type versus *dhc-1* mutant embryos (Supplemental Table s3). During the ensuing mitosis in wild type, the posterior centrosome moved at a net rate of 0.067 ± 0.005 μm/s to a position 9.9 ± 0.6 μm from the posterior cortex. In *dhc-1* ts mutant embryos, that rate was modestly reduced (0.056 ± 0.010 for c*t76*; 0.048 ± 0.013 for *or195*; Supplemental Table s3), but the final position of the posterior centrosome was similar to wild type. Thus, either residual DHC-1 function in *dhc-1* ts mutant embryos is sufficient for the posterior spindle shift, or DHC-1 is not the primary motor for that movement.

Fast Temperature-Shift Analysis of DHC-1 Function in Rotation of the Centrosome/Nucleus Complex

Although the preceding tests of DHC-1 function were informative, the time delay between initiation of DHC-1 inhibition and analysis of events in embryos was 24 h. A process of interest might be influenced indirectly by defects in processes that preceded it. As noted above, RNAi depletion of DHC-1 can compromise the maternal germline sufficiently

Table 2. Summary of defects observed in *dhc-1 (RNAi)* and *dhc-1* mutant embryos.

maternal genotype	% of embryos that underwent normal vs. mildly defective vs. severely defective:																
	pronuclear migration[a]				centrosome rotation[b]				spindle formation[c]			anaphase[d]			cytokinesis[e]		
	normal	mild	severe	ND	normal	mild	severe	ND	normal	mild	severe	normal	mild	severe	normal	mild	severe
wild type n=10	100	0	0		100	0	0		100	0	0	100	0	0	100	0	0
dhc-1(RNAi) n=10	10	20	70		0	0	10	90	0	10	90	0	10	90	0	50	50
dhc-1(ct76)/+ n=16	6	88	6		6	44	44	6	0	50	50	0	0	100	0	0	100
dhc-1(or195)/hDf6 n=10	0	70	0	30	10	20	60	10	0	30	70	0	0	100	0	0	100
dhc-1(or195) n=19	26	74	0		10	43	37	10	0	37	63	10	0	90	10	37	53
dhc-1(ct77)/+ n=10	0	100	0		60	10	10	20	0	100	0	80	10	10	40	30	30
dhc-1(ct42)/+ n=10	20	80	0		40	20	20	20	0	100	0	60	20	20	30	40	30
dhc-1(sb42)/+ n=10	100	0	0		40	60	0		10	90	0	100	0	0	100	0	0
dhc-1(h482) n=10	100	0	0		80	20	0		40	60	0	100	0	0	50	50	0

Wild-type and mutant L4 hermaphrodites were incubated at 25°C for 24 hr. Embryos from these mothers were then scored for defects in different events during the first cell cycle. For RNAi, adult hermaphrodites were injected with *dhc-1* dsRNA, and embryos from injected mothers were scored for defects 18-24 hours after injection. ND, not determined; n, number of embryos scored.

[a] Pronuclear migration: normal, sperm and oocyte pronuclei migrated and met in the posterior hemisphere of the embryo; mild, pronuclei migrated more slowly and met more centrally than in wild type; severe, pronuclei failed to meet prior to NEB; ND, imaging of embryos was initiated after pronuclear migration.

[b] Centrosome/nucleus complex rotation: normal, rotation of the centrosome/nucleus complex prior to NEB; mild, delay in rotation or partial rotation; severe, no rotation; ND, centrosomes were not visible or the orientation of the centrosome/nucleus complex did not allow rotation to be assessed.

[c] Spindle formation: normal, formation of a properly oriented and normal-sized bipolar spindle; mild, bipolar spindle was misoriented; severe, spindle was misoriented and partially collapsed, monopolar, or failed to form.

[d] Anaphase: normal, separation of two chromosome masses of equal size and formation of a single nucleus in each daughter cell; mild, formation of nuclei of unequal size or multiple nuclei in the daughter cells; severe, chromosomes failed to separate and multiple micronuclei formed.

[e] Cytokinesis: normal, formation of a larger anterior cell and a smaller posterior cell; mild, blebbing occured, and cytokinesis produced daughter cells that were more or less asymmetric than in wild type; severe, cleavage furrow failed to completely invaginate.

that it stops producing oocytes. The background physiology of embryos analyzed before that shutdown is probably abnormal to some degree. A more obvious problem is that spindle assembly defects preclude meaningful assessment of dynein's involvement in chromosome congression and segregation. In hopes of circumventing these problems, we tested how quickly phenotypes occurred in *dhc-1* ts mutants after a temperature upshift. To allow direct observation during a temperature shift, a temperature-controlled microscope stage was built (Supplemental Figure s1). With two solid-state heat pumps controlling the slide temperature, it was possible to drive embryos from 16 to 25°C in ~30 s during observation with an oil immersion objective. *dhc-1* ts mutant embryos (*ct76*, *or195*, and *ct77-ct42*) showed mutant phenotypes (e.g., cortical blebbing and spindle collapse) within 60 s of initiation of such an upshift. In additional tests of *ct76*, a fast upshift to 25°C that prevented spindle assembly and cytokinesis in P_0 followed by a downshift to 16°C allowed mitosis and cytokinesis to occur during the second cell cycle. Thus, with at least one ts allele, thermal inhibition of DHC-1 function could be reversed.

With the thermal stage, we first addressed the question of whether DHC-1 has a direct role in rotation of the centrosome/nucleus complex in the first two cell cycles. In all *dhc-1* ts mutant embryos observed at 16°C, centrosomes separated normally and then established a mitotic spindle along the AP axis (n = 11) (Figure 4C and Videos 3 and 7). In *ct76* embryos that showed normal transverse centrosome separation (n = 9), an upshift at the moment of pronuclear meeting prevented rotation of the centrosome axis onto the AP axis (our unpublished data). In *or195* embryos (n = 10), an upshift at pronuclear meeting prevented rotation in eight cases (Figure 5B, d, and Video 8). In the other two cases, rotation was partial (~45°). Transverse spindles in *or195* embryos eventually did rotate onto the AP axis, when one or the other spindle pole was pulled toward the posterior cortex during anaphase (Figure 5B, e and f). These results show that inhibition of DHC-1 has a direct effect on rotation of the P_0 centrosome-centrosome axis, consistent with a mechanism in which dynein-mediated pulling forces on microtubules emanating from one or both centrosomes drive that rotation.

The influence of dynein on rotation of the centrosome axis also was studied in P_1. The smaller size of P_1 and variations in the geometry of centrosome separation in wild type made observation of centrosomes and the timing of upshifts more difficult with DIC microscopy. Furthermore, in both wild-

type and *ct76* embryos held at 16°C, P_1 centrosome separation sometimes occurred directly along the AP axis. To facilitate well timed upshifts immediately after transverse centrosome separation, we generated a *ct76* strain expressing GFP::β-tubulin (Figure 5, A and C). When *ct76* embryos were shifted to 25°C immediately after transverse P_1 centrosome separation, rotation always failed (n = 12) (Figure 5C, c–e, and Video 9). Because the first mitotic midbody is thought to provide a cue for rotation of the centrosome axis in P_1, it is noteworthy that the *ct76* embryos described above had completed cytokinesis and had a normally positioned midbody before the temperature shift. These results, along with the transient accumulation of DHC-1 observed along the AB-P_1 boundary (Figure 2D), support the hypothesis of Skop and White that dynein-dynactin anchored to the anterior cortex of P_1 generates the force for centrosome axis rotation (Skop and White, 1998).

Fast Temperature-Shift Analysis of DHC-1 Function in Mitosis

Cytoplasmic dynein has been proposed to contribute to multiple processes during mitosis, including chromosome congression and silencing of the kinetochore-dependent spindle checkpoint by means of transporting checkpoint proteins from kinetochores to spindle poles (Savoian *et al*., 2000; Sharp *et al*., 2000b; Howell *et al*., 2001; reviewed in McIntosh *et al*., 2002). To test those hypotheses, *ct76* and *or195* embryos containing GFP-tagged histone H2B were subjected to fast upshifts immediately after NEB. Although earlier upshifts prevented spindle assembly, post-NEB upshifts allowed formation of what appeared to be normal bipolar spindles (Video 7). After the upshift, chromosomes in *ct76* and *or195* embryos congressed toward the spindle equator but then failed to form a tight metaphase plate (Figure 6, C and D; compare Videos 10–12). Anaphase commonly resulted in lagging chromosomes (Figure 6C, e and f; Figure 6D, e; and Videos 11 and 12). Even when the upshift was delayed until the initial phase of chromosome congression was mostly completed, metaphase plates were irregular, rather than linear and well focused (Figure 6E, d, and Video 13). These results suggest that minus-end–directed forces generated by cytoplasmic dynein contribute to prometaphase-metaphase chromosome orientation and alignment, which is critical in preventing or correcting merotelic chromosome attachments that result in single chromosomes being stretched between separating spindle poles during anaphase (Powers *et al*., 2004).

If dynein contributes to silencing the kinetochore-dependent checkpoint, one would expect dynein inhibition to delay anaphase. At 16°C, the interval between NEB and the beginning of anaphase was slightly shorter for wild-type than for *ct76* embryos (238 ± 38 and 284 ± 51 s, respectively; n = 10 for each; Supplemental Table s3). For wild-type embryos at 25°C that interval decreased to 158 ± 37 s (n = 10). For *ct76* and *or195* embryos upshifted to 25°C at or just after NEB, the interval increased dramatically to 583 ± 174 s (n = 6) and 340 ± 110 s (n = 6), respectively (compare Videos 10–12). It is unlikely that this anaphase delay resulted from the chromosome congression/orientation defects just described, because similar defects caused by KLP-19 inhibition do not cause anaphase delays (Powers *et al*., 2004). These observations, along with the findings of Encalada *et al*. (2004), suggest that DHC-1 contributes to silencing of a kinetochore-dependent spindle checkpoint in *C. elegans* embryos, as has been suggested for other organisms (Howell *et al*., 2001; McIntosh *et al*., 2002).

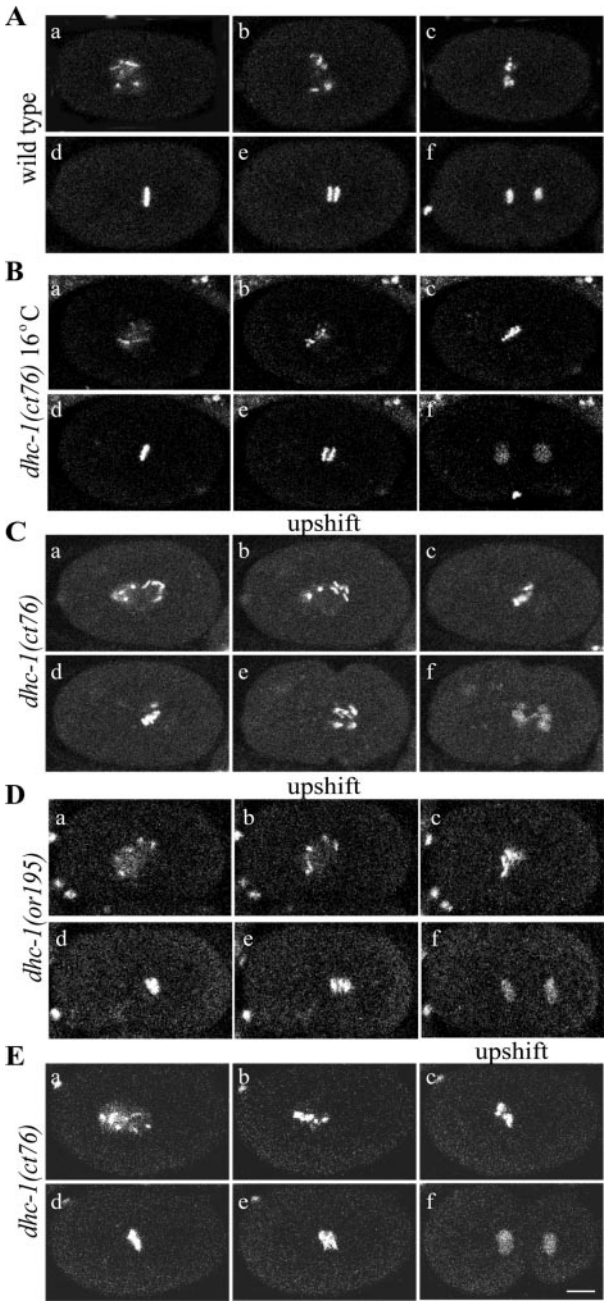

Figure 6. Defects in chromosome congression in *dhc-1* embryos upshifted during prometaphase. Time-lapse confocal images show embryos expressing GFP::histone. (A and Video 10) In wild-type embryos incubated at either 16 or 25°C, chromosomes congressed to form a tight metaphase plate (d) and segregated to form two discrete and well ordered groups (e and f). (B) In *dhc-1(ct76)* mutant embryos maintained at 16°C, chromosome congression (c and d) and segregation (e and f) looked normal. (C and Video 11) In *dhc-1(ct76)* mutant embryos shifted from 16 to 25°C at NEB, chromosomes congressed poorly (c and d), chromosomes lagged during anaphase (e), and segregation was defective (e and f). (D and Video 12) In *dhc-1(or195)* mutant embryos shifted from 16 to 25°C at NEB, chromosome congression was defective (c and d) and some chromosomes lagged in early anaphase (e), but segregation was better than in *ct76* embryos (f). (E and Video 13) In *dhc-1(ct76)* embryos shifted from 16 to 25°C in late prometaphase during congression, chromosomes did not fully congress to a tight metaphase plate (d). Some lagging chromosomes were observed in early anaphase (e), but the subsequent extent of separation and cytokinesis seemed normal (f). Bar, 10 μm.

Different experimental systems have provided conflicting results about whether cytoplasmic dynein generates force that moves chromosomes apart during anaphase (see *Discussion*). In *C. elegans* embryos, chromosome segregation is accomplished solely by anaphase B pole separation (Oegema *et al*., 2001), during which the anterior pole remains relatively stationary, while the posterior pole moves toward the posterior cortex. The spindle severing experiments of Grill *et al*. (2001) suggest that this pole movement is driven by cortical forces that pull most strongly on astral microtubules attached to the posterior spindle pole. Cortically anchored dynein is a good candidate for that cortical force generator. However, our tests with the *dhc-1* ts mutants do not provide support for this idea. In ts mutant embryos with spindles oriented along the AP axis, the posterior spindle pole moved to a normal posterior position, although at a somewhat reduced rate (see above; Supplemental Table s3). In ts mutant embryos with bipolar spindles set up transverse to the AP axis, at least one spindle pole moved toward the posterior during anaphase (Figure 5B) (n = 19). In more severe cases, when ts mutant embryos had monopolar or collapsed spindles, the entire spindle moved toward the posterior cortex (Figure 4D) (n = 14). Finally, *ct76* and *or195* embryos upshifted during prometaphase, well before the onset of anaphase, showed fairly normal anaphase chromosome separation (Figure 6, C and D, and Videos 11 and 12). This was quantified by measuring the final distance between the centers of decondensing chromosome masses during telophase (wild-type = 4.7 ± 0.3 μm [n = 9]; *ct76* = 4.8 ± 0.5 μm [n = 9], p = 0.8; *or195* = 5.1 ± 0.4 μm [n = 6], p = 0.09). Thus, although these alleles are not completely null, they suggest that cytoplasmic dynein is dispensable during anaphase spindle pole separation in *C. elegans* embryos. Other possible mechanisms for generating posterior cortical force include minus-end–directed kinesins and tethered microtubule depolymerization.

DISCUSSION

Because cytoplasmic dynein contributes to so many processes, pursuing questions about its specific functions with approaches that cause a gradual loss of function has left gaps in our understanding. The conditional *dhc-1* alleles we have characterized allow both long-term and very rapid inhibition of the motor subunit of dynein. Direct observation of cellular/developmental processes of interest during rapid inhibition allows focused analysis of specific dynein functions, minimizing complications due to earlier requirements and the potential for indirect effects.

Insights into Functions of DHC-1 during C. elegans Early Embryonic Development

Spindle Alignment. Because the position and orientation of the mitotic spindle dictate the pattern of cell division and segregation of components to daughter cells (reviewed in White and Strome, 1996), alignment of the spindle is tightly regulated in many developing organisms. Studies in yeast, *Drosophila*, *C. elegans*, and mammalian cells have implicated dynein in spindle alignment (Eschel *et al*., 1993; Li *et al*., 1993; McGrail and Hays, 1997; Skop and White, 1998; Gönczy *et al*., 1999; O'Connell and Wang, 2000). In *C. elegans*, RNAi depletion of DNC-1 or DNC-2, two components of dynactin, or partial RNAi depletion of DHC-1 impaired the 90° rotation of the centrosome/nucleus complex that is required to correctly align the mitotic spindle in the P_0 and P_1 blastomeres (Skop and White, 1998; Gönczy *et al*., 1999). Because of the gradual depletion caused by RNAi, the possibility of indirect effects was not eliminated.

Our studies of fast-acting ts *dhc-1* mutations and DHC-1 location provide strong support for the direct involvement of dynein in rotation: rotation did not occur in ts mutant embryos upshifted just before rotation in P_0 or P_1. Hyman and White (Hyman and White, 1987; Hyman, 1989) demonstrated that the rotation in P_1 is mediated by an interaction of astral microtubules with a site on the anterior cortex. We observed a transient accumulation of DHC-1 along the anterior cortex of P_1 during the period of rotation, similar to that observed for DNC-1 (Skop and White, 1998), consistent with the hypothesis that dynein/dynactin tethered to the anterior cortex captures and reels in microtubules emanating from one centrosome. By analogy to P_1, dynein anchored to the anterior cortex of P_0 may capture astral microtubules and pull on them to mediate rotation of the centrosome/nucleus complex in that cell as well. An alternative model for P_0, suggested by analysis of *let-99* mutant embryos (Tsou *et al*., 2002), is that dynein-generated pulling forces are distributed around the entire cortex but are attenuated at posterior-lateral sites by LET-99 protein. Our results do not discriminate between the "localized dynein" and "broadly distributed dynein with localized attenuation" models. They might be distinguished via spatially restricted thermal inactivation of ts DHC-1 by irradiation of specific cortical regions with a heat-generating microbeam of light.

Chromosome Congression. Dynein has been identified as a kinetochore component in numerous cell types (Pfarr *et al*., 1990; Steuer *et al*., 1990; Starr *et al*., 1998; Sharp *et al*., 2000b), consistent with a role in mitotic chromosome movement. Previous experiments have produced conflicting views of dynein function during prometaphase. Inhibition of dynein in *Drosophila* and mammalian cells by a variety of methods, including genetic mutations, RNAi, antibody injection, and overexpression of dynamitin, in some cases caused chromosome congression defects and in other cases did not. In *Drosophila*, congression defects included a reduced rate of poleward chromosome movement during prometaphase (Savoian *et al*., 2000) and a failure of kinetochore alignment at metaphase (Sharp *et al*., 2000b); congression defects were not observed by Starr *et al*. (1998) or Goshima and Vale (2003). In mammalian systems, Echeverri *et al*. (1996) observed defects in chromosome alignment in COS-7 cells, whereas Howell *et al*. (2001) did not observe congression defects in PtK1 cells. In our experiments, DHC-1 inhibition at NEB or later in prometaphase consistently caused disordered metaphase plates, revealing that in *C. elegans* DHC-1 does contribute to chromosome congression. The congression defects may be due to impaired dynein-dependent force generation at the kinetochore or to altered spindle microtubule dynamics and organization.

Anaphase. Studies of dynein contributions to anaphase in other systems have often been complicated by the requirement for dynein in spindle assembly (Robinson *et al*., 1999) and have produced conflicting results. For example, injection of dynein inhibitors into *Drosophila* embryos disrupted both poleward chromosome movement (anaphase A) and spindle pole separation (anaphase B) (Sharp *et al*., 2000a,b). Also in *Drosophila*, mutations in *zw10*, which disrupt dynein localization to kinetochores but do not otherwise impair spindle structure, caused reduced rates of poleward chromosome movement, lagging chromosomes, and segregation defects (Starr *et al*., 1998; Savoian *et al*., 2000). In contrast, RNAi depletion of dynein from *Drosophila* S2 cells caused a

delay in the metaphase-to-anaphase transition, but did not impair chromosome segregation (Goshima and Vale, 2003). Similarly, inhibition of dynein function in PtK1 cells affected spindle checkpoint inactivation but did not impair chromosome segregation during anaphase (Howell *et al*., 2001). Thus, whether dynein contributes directly to anaphase chromosome separation remains controversial.

Two aspects of anaphase in *C. elegans* are unusual and intriguing. First, chromosome segregation is accomplished solely by spindle pole separation (anaphase B) (Oegema *et al*., 2001). Thus, a role for dynein in anaphase A chromosome-to-pole movement is not an issue. Second, anaphase B spindle pole separation seems to be driven primarily by cortical pulling forces on astral microtubules (Grill *et al*., 2001) with little or no contribution from pushing forces by antiparallel microtubules in the spindle interzone. In fact, the *C. elegans* interzone may actually resist pole separation (Grill *et al*., 2001; Saunders and Saxton, unpublished data). The cortical pulling forces are stronger toward the posterior than toward the anterior (Grill *et al*., 2001, 2003). Thus, anaphase B is accomplished primarily by movement of the posterior spindle pole toward the posterior cortex. This movement also positions the spindle asymmetrically, leading to an unequal first division, which is critical for subsequent normal development.

Dynein, tethered at the posterior cortex, has been a prime candidate for the posterior cortical pulling motor. Our studies of spindle movements in upshifted *dhc-1* ts mutant embryos do not support such a role for dynein. All upshifted *dhc-1* embryos that we analyzed displayed robust posterior movement of the spindle during anaphase. Mutant embryos containing a bipolar spindle displayed posterior migration of one or both spindle poles. Monopolar spindles, too, underwent posterior movement. Furthermore, anaphase chromosome separation was achieved by ts mutant embryos upshifted after they had well-formed bipolar spindles. Thus, either dynein is not the posterior pulling motor, or adequate pulling forces can be generated by residual dynein function in the upshifted ts mutants. The accumulation of DHC-1 on centrosomes and spindle poles in ts mutant embryos suggests that mutant DHC-1 might be capable of translocating along microtubules to their minus ends and fail to release. So, mutant DHC-1 tethered to the cortex could retain the ability to capture and reel in astral microtubules during anaphase. Arguing against retention of the ability to generate cortical pulling forces, at least by the more severe ts mutants, is the fact that they are unable to pull on astral microtubules during rotation of the centrosome/nucleus complex.

In wild-type embryos, anaphase B movement of the posterior spindle pole is accompanied by dramatic lateral oscillations and followed by flattening of the centrosome. Gotta and Ahringer (2001) observed that all three events require G protein function, consistent with the general assumption that posterior-directed movement, oscillations, and flattening of the posterior spindle pole are mechanistically linked, perhaps by a single force-producing mechanism. Our analysis of ts *dhc-1* mutants suggests otherwise. The five most severe *dhc-1* ts mutations caused a marked reduction or complete absence of oscillations and centrosome flattening at both 16 and 25°C, but posterior-directed anaphase movement of the spindle occurred (e.g., compare Videos 3 and 7 with Video 1). Severson and Bowerman (2003) observed similar results in embryos partially depleted of DHC-1 by RNAi. This demonstrates that the lateral oscillations and flattening are not causally linked to posterior-directed spindle migration. This suggests different force-generating mechanisms; oscillations and centrosome flattening require normal DHC-1 activity, whereas the posterior spindle shift requires little or none.

Lesions in the ts Variants of DHC-1

The DHC motor domain contains six AAA domains (reviewed in King, 2000; Vale, 2000), four that contain a complete P-loop motif (1–4) and two that do not (5 and 6). The current view is that AAA1 is the critical domain for ATP hydrolysis, AAA3 binds but may not hydrolyze ATP, and AAA2 and AAA4 have structural rather than nucleotide-binding roles (King, 2000; Silvanovich *et al*., 2003; Reck-Peterson and Vale, 2004). The three lesions identified thus far in *C. elegans dhc-1* mutants alter amino acids in AAA2, AAA3, and AAA4. The dominant *ct76* mutation, which is the most severe allele, causes an Ala-to-Asp change in the Box VI region in AAA4. The recessive *or195* mutation, which is the next most severe allele, causes a His-to-Leu change six residues upstream from the AAA2 P-loop (Hamill *et al*., 2002). Because ATP binding by AAA2 and AAA4 does not occur or is not important for dynein function, it is likely that the *or195* and *ct76* lesions cause either local defects in folding of their respective AAA domains or longer range defects in structural relationships between domains. The dominant *ct42* and *ct77* alleles cause a Gly-to-Glu substitution in the fourth residue of the P-loop in AAA3. This confirms the in vivo importance of the AAA3 P-loop and raises the possibility that the long negative side chain of glutamic acid alters ATP binding at nonpermissive temperature. All three dominant alleles behave genetically as gain-of-function poisons with phenotypes sensitive to mutant versus wild-type gene dosage (Mains *et al*., 1990). This raises the question of how the mutant DHC-1 proteins inactivate wild-type protein. Because the cytoplasmic dynein complex incorporates two DHC subunits, as well as a number of associated proteins, it is possible that the presence of one mutant DHC in a complex is sufficient to dramatically impair force-producing interactions of the motor domains with microtubules, causing binding to be either too weak or too strong. The poison effect could mean that cytoplasmic dynein is an obligate two-headed motor and that the presence of one "motor dead" subunit eliminates critical processivity. However, the *or195* ts mutation in AAA2 is recessive. Furthermore, all of the many nonconditional *dhc-1/let-354* alleles are recessive. This indicates that the poison effects of the *ct76* and *ct42-ct77* alleles are allele-specific. Future structural and kinetic investigation will provide insights into the functional relationship between the two heads.

The prospects for using the Gly-to-Glu P-loop mutation to create fast-acting temperature-sensitive mutations in other dyneins are good. The sequence of the AAA3 P-loop is completely conserved in all known DHCs, and engineering the Gly-to-Glu change into *S. cerevisiae* DHC1 did cause a dominant ts dynein phenotype. It is noteworthy that, when no wild-type gene is present, the *ct42-ct77* lesion in worms and yeast causes a nonconditional mutant phenotype. Thus, the ts P-loop mutation does not allow completely normal dynein function at permissive temperature. However, it is tantalizing to consider that creating fast-acting ts dynein mutants in other model systems and cells could help address a number of central questions about mitosis, cytoplasmic transport, and axoneme bending. Furthermore, the Gly-to-Glu or similar mutations also could be effective in kinesins, myosins, G proteins, and a variety of other P-loop proteins, allowing time-resolved function-disruption studies. Issues that will likely impact the success of this approach are temperature range of the organism and oligomerization

state of the target protein. Our preliminary tests indicate that the Gly-to-Glu mutation does render a *Drosophila* dimeric kinesin ts, and we are preparing to test monomeric P-loop proteins.

ACKNOWLEDGMENTS

We are especially grateful to Paul Mains, Danielle Hamill, Bruce Bowerman, and Ann Rose for sharing *dhc-1* alleles and information with us. We thank Alan Bender, Kerry Bloom, Arshad Desai, Margaret Fuller, Pierre Gönczy, Tony Hyman, Yoji Kohara, Chris Malone, John White, and Haining Zhang for reagents; Adam Saunders for help with some strain constructions; Aaron Pilling for the NIH Image tracking macro; Lynda Delph for assistance with statistics; Jon Henry for building the temperature-controlled stage; and members of the Strome and Saxton laboratories for discussions and ideas. This research was supported by National Institutes of Health grants GM58811 (to W.M.S. and S. S.) and GM34059 (to S. S.)

REFERENCES

Asai, D. J., and Koonce, M. P. (2001). The dynein heavy chain: structure, mechanics and evolution. Trends Cell Biol. *11*, 196–202.

Brenner, S. (1974). The genetics of *Caenorhabditis elegans*. Genetics *77*, 71–94.

Consortium, T. C. e. S. (1998). Genome sequence of the nematode *C. elegans*: a platform for investigating biology. Science *282*, 2012–2018.

Deyrup, A. T., Krishnan, S., Cockburn, B. N., and Schwartz, N. B. (1998). Deletion and site-directed mutagenesis of the ATP-binding motif (P-loop) in the bifunctional murine ATP-sulfurylase/adenosine 5′-phosphosulfate kinase enzyme. J. Biol. Chem. *273*, 9450–9456.

Encalada, S. E., Willis, J., Lyczak, R., and Bowerman, B. (2004). A spindle checkpoint functions during mitosis in the early *Caenorhabditis elegans* embryo. Mol. Biol. Cell *16*, 1056–1070.

Eshel, D., Urrestarazu, L. A., Vissers, S., Jauniaux, J. C., van Vliet-Reedijk, J. C., Planta, R. J., and Gibbons, I. R. (1993). Cytoplasmic dynein is required for normal nuclear segregation in yeast. Proc. Natl. Acad. Sci. USA *90*, 11172–11176.

Gee, M. A., Heuser, J. E., and Vallee, R. B. (1997). An extended microtubule-binding structure within the dynein motor domain. Nature *390*, 636–639.

Gepner, J., Li, M., Ludmann, S., Kortas, C., Boylan, K., Iyadurai, S. J., McGrail, M., and Hays, T. S. (1996). Cytoplasmic dynein function is essential in *Drosophila melanogaster*. Genetics *142*, 865–878.

Gibbons, I. R. (1995). Dynein family of motor proteins: present status and future questions. Cell Motil. Cytoskeleton *32*, 136–144.

Gibbons, I. R., Gibbons, B. H., Mocz, G., and Asai, D. J. (1991). Multiple nucleotide-binding sites in the sequence of dynein beta heavy chain. Nature *352*, 640–643.

Gönczy, P., Pichler, S., Kirkham, M., and Hyman, A. A. (1999). Cytoplasmic dynein is required for distinct aspects of MTOC positioning, including centrosome separation, in the one cell stage *Caenorhabditis elegans* embryo. J. Cell Biol. *147*, 135–150.

Goshima, G., and Vale, R. D. (2003). The roles of microtubule-based motor proteins in mitosis: comprehensive RNAi analysis in the *Drosophila* S2 cell line. J. Cell Biol. *162*, 1003–1016.

Gotta, M., and Ahringer, J. (2001). Distinct roles for Gα and G$\beta\gamma$ in regulating spindle position and orientation in *Caenorhabditis elegans* embryos. Nat. Cell Biol. *3*, 297–300.

Grill, S. W., Gönczy, P., Stelzer, E. H., and Hyman, A. A. (2001). Polarity controls forces governing asymmetric spindle positioning in the *Caenorhabditis elegans* embryo. Nature *409*, 630–633.

Grill, S. W., Howard, J., Schaffer, E., Stelzer, E. H., and Hyman, A. A. (2003). The distribution of active force generators controls mitotic spindle position. Science *301*, 518–521.

Hamill, D. R., Severson, A. F., Carter, J. C., and Bowerman, B. (2002). Centrosome maturation and mitotic spindle assembly in *C. elegans* require SPD-5, a protein with multiple coiled-coil domains. Dev. Cell *3*, 673–684.

Harada, A., Takei, Y., Kanai, Y., Tanaka, Y., Nonaka, S., and Hirokawa, N. (1998). Golgi vesiculation and lysosome dispersion in cells lacking cytoplasmic dynein. J. Cell Biol. *141*, 51–59.

Hoffman, D. B., Pearson, C. G., Yen, T. J., Howell, B. J., and Salmon, E. D. (2001). Microtubule-dependent changes in assembly of microtubule motor proteins and mitotic spindle checkpoint proteins at PtK1 kinetochores. Mol. Biol. Cell *12*, 1995–2009.

Howell, A. M., and Rose, A. M. (1990). Essential genes in the *hDf6* region of chromosome I in *Caenorhabditis elegans*. Genetics *126*, 583–592.

Howell, B. J., McEwen, B. F., Canman, J. C., Hoffman, D. B., Farrar, E. M., Rieder, C. L., and Salmon, E. D. (2001). Cytoplasmic dynein/dynactin drives kinetochore protein transport to the spindle poles and has a role in mitotic spindle checkpoint inactivation. J. Cell Biol. *155*, 1159–1172.

Hyman, A. A. (1989). Centrosome movement in the early divisions of *Caenorhabditis elegans*: a cortical site determining centrosome position. J. Cell Biol. *109*, 1185–1193.

Hyman, A. A., and White, J. G. (1987). Determination of cell division axes in the early embryogenesis of *Caenorhabditis elegans*. J. Cell Biol. *105*, 2123–2135.

Kamath, R. S., Martinez-Campos, M., Zipperlen, P., Fraser, A. G., and Ahringer, J. (2001). Effectiveness of specific RNA-mediated interference through ingested double-stranded RNA in *Caenorhabditis elegans*. Genome Biol. *2*, RESEARCH0002.

King, S. M. (2000). AAA domains and organization of the dynein motor unit. J. Cell Sci. *113*, 2521–2526.

Koonce, M. P. (1997). Identification of a microtubule-binding domain in a cytoplasmic dynein heavy chain. J. Biol. Chem. *272*, 19714–19718.

Kull, F. J., Sablin, E. P., Lau, R., Fletterick, R. J., and Vale, R. D. (1996). Crystal structure of the kinesin motor domain reveals a structural similarity to myosin. Nature *380*, 550–555.

Li, Y. Y., Yeh, E., Hays, T., and Bloom, K. (1993). Disruption of mitotic spindle orientation in a yeast dynein mutant. Proc. Natl. Acad. Sci. USA *90*, 10096–10100.

Lye, R. J., Wilson, R. K., and Waterston, R. H. (1995). Genomic structure of a cytoplasmic dynein heavy chain gene from the nematode *Caenorhabditis elegans*. Cell Motil. Cytoskeleton *32*, 26–36.

Mains, P. E., Sulston, I. A., and Wood, W. B. (1990). Dominant maternal-effect mutations causing embryonic lethality in *Caenorhabditis elegans*. Genetics *125*, 351–369.

McGrail, M., and Hays, T. S. (1997). The microtubule motor cytoplasmic dynein is required for spindle orientation during germline cell divisions and oocyte differentiation in *Drosophila*. Development *124*, 2409–2419.

McIntosh, J. R., Grishchuk, E. L., and West, R. R. (2002). Chromosome-microtubule interactions during mitosis. Annu. Rev. Cell Dev. Biol. *18*, 193–219.

Milisav, I. (1998). Dynein and dynein-related genes. Cell Motil. Cytoskeleton *39*, 261–272.

Mitenko, N. L., Eisner, J. R., Swiston, J. R., and Mains, P. E. (1997). A limited number of *Caenorhabditis elegans* genes are readily mutable to dominant, temperature-sensitive maternal-effect embryonic lethality. Genetics *147*, 1665–1674.

O'Connell, C. B., and Wang, Y. L. (2000). Mammalian spindle orientation and position respond to changes in cell shape in a dynein-dependent fashion. Mol. Biol. Cell *11*, 1765–1774.

Oegema, K., Desai, A., Rybina, S., Kirkham, M., and Hyman, A. A. (2001). Functional analysis of kinetochore assembly in *Caenorhabditis elegans*. J. Cell Biol. *153*, 1209–1226.

Ogawa, K. (1991). Four ATP-binding sites in the midregion of the beta heavy chain of dynein. Nature *352*, 643–645.

Ogawa, K., and Mohri, H. (1996). A dynein motor superfamily. Cell Struct. Funct. *21*, 343–349.

Paschal, B. M., Shpetner, H. S., and Vallee, R. B. (1987). MAP 1C is a microtubule-activated ATPase which translocates microtubules in vitro and has dynein-like properties. J. Cell Biol. *105*, 1273–1282.

Pfarr, C. M., Coue, M., Grissom, P. M., Hays, T. S., Porter, M. E., and McIntosh, J. R. (1990). Cytoplasmic dynein is localized to kinetochores during mitosis. Nature *345*, 263–265.

Powers, J., Rose, D. J., Saunders, A., Dunkelbarger, S., Strome, S., and Saxton, W. M. (2004). Loss of KLP-19 polar ejection force causes misorientation and missegregation of holocentric chromosomes. J. Cell Biol. *166*, 991–1001.

Reck-Peterson, S. L., and Vale, R. D. (2004). Molecular dissection of the roles of nucleotide binding and hydrolysis in dynein's AAA domains in *Saccharomyces cerevisiae*. Proc. Natl. Acad. Sci. USA *101*, 1491–1495.

Robinson, J. T., Wojcik, E. J., Sanders, M. A., McGrail, M., and Hays, T. S. (1999). Cytoplasmic dynein is required for the nuclear attachment and migration of centrosomes during mitosis in *Drosophila*. J. Cell Biol. *146*, 597–608.

Salina, D., Bodoor, K., Eckley, D. M., Schroer, T. A., Rattner, J. B., and Burke, B. (2002). Cytoplasmic dynein as a facilitator of nuclear envelope breakdown. Cell *108*, 97–107.

Sambrook, J., Fritsch, E. F., and Maniatis, T. (1982). Molecular Cloning: A Laboratory Manual, Cold Spring Harbor, NY: Cold Spring Harbor Laboratory Press.

Savoian, M. S., Goldberg, M. L., and Rieder, C. L. (2000). The rate of poleward chromosome motion is attenuated in *Drosophila zw10* and *rod* mutants. Nat. Cell Biol. *2*, 948–952.

Sawin, K. E., and Scholey, J. M. (1991). Motor proteins in cell division. Trends Cell Biol. *1*, 122–129.

Severson, A. F., and Bowerman, B. (2003). Myosin and the PAR proteins polarize microfilament-dependent forces that shape and position mitotic spindles in *Caenorhabdities elegans*. J. Cell Biol. *161*, 21–26.

Sharp, D. J., Brown, H. M., Kwon, M., Rogers, G. C., Holland, G., and Scholey, J. M. (2000a). Functional coordination of three mitotic motors in *Drosophila* embryos. Mol. Biol. Cell *11*, 241–253.

Sharp, D. J., Rogers, G. C., and Scholey, J. M. (2000b). Cytoplasmic dynein is required for poleward chromosome movement during mitosis in *Drosophila* embryos. Nat. Cell Biol. *2*, 922–930.

Shen, H., Yao, B. Y., and Mueller, D. M. (1994). Primary structural constraints of P-loop of mitochondrial F1-ATPase from yeast. J. Biol. Chem. *269*, 9424–9428.

Silvanovich, A., Li, M. G., Serr, M., Mische, S., and Hays, T. S. (2003). The third P-loop domain in cytoplasmic dynein heavy chain is essential for dynein motor function and ATP-sensitive microtubule binding. Mol. Biol. Cell *14*, 1355–1365.

Skop, A. R., and White, J. G. (1998). The dynactin complex is required for cleavage plane specification in early *Caenorhabditis elegans* embryos. Curr. Biol. *8*, 1110–1116.

Starr, D. A., Williams, B. C., Hays, T. S., and Goldberg, M. L. (1998). ZW10 helps recruit dynactin and dynein to the kinetochore. J. Cell Biol. *142*, 763–774.

Steuer, E. R., Wordeman, L., Schroer, T. A., and Sheetz, M. P. (1990). Localization of cytoplasmic dynein to mitotic spindles and kinetochores. Nature *345*, 266–268.

Strome, S., Powers, J., Dunn, M., Reese, K., Malone, C. J., White, J., Seydoux, G., and Saxton, W. M. (2001). Spindle dynamics and the role of γ-tubulin in early *Caenorhabditis elegans* embryos. Mol. Biol. Cell *12*, 1751–1764.

Strome, S., and Wood, W. B. (1983). Generation of asymmetry and segregation of germ-line granules in early *C. elegans* embryos. Cell *35*, 15–25.

Tsou, M. B., Hayashi, A., DeBella, L. R., McGrath, G., and Rose, L. S. (2002). LET-99 determines spindle position and is asymmetrically enriched in response to PAR polarity cues in *C. elegans* embryos. Development *129*, 4469–4481.

Vaisberg, E. A., Koonce, M. P., and McIntosh, J. R. (1993). Cytoplasmic dynein plays a role in mammalian mitotic spindle formation. J. Cell Biol. *123*, 849–858.

Vale, R. D. (2000). AAA proteins. Lords of the ring. J. Cell Biol. *150*, F13–19.

Vale, R. D. (2003). The molecular motor toolbox for intracellular transport. Cell *112*, 467–480.

Vallee, R. B., and Hook, P. (2003). Molecular motors: a magnificent machine. Nature *421*, 701–702.

Verdon, G., Albers, S. V., Dijkstra, B. W., Driessen, A. J., and Thunnissen, A. M. (2003). Crystal structures of the ATPase subunit of the glucose ABC transporter from *Sulfolobus solfataricus*: nucleotide-free and nucleotide-bound conformations. J. Mol. Biol. *330*, 343–358.

Walhout, A. J., and Vidal, M. (2001). High-throughput yeast two-hybrid assays for large-scale protein interaction mapping. Methods *24*, 297–306.

Walker, J. E., Saraste, M., Runswick, M. J., and Gay, N. J. (1982). Distantly related sequences in the α- and β-subunits of ATP synthase, myosin, kinases and other ATP-requiring enzymes and a common nucleotide binding fold. EMBO J. *1*, 945–951.

White, J., and Strome, S. (1996). Cleavage plane specification in *C. elegans*: how to divide the spoils. Cell *84*, 195–198.

Wicks, S. R., de Vries, C. J., van Luenen, H. G., and Plasterk, R. H. (2000). CHE-3, a cytosolic dynein heavy chain, is required for sensory cilia structure and function in *Caenorhabditis elegans*. Dev. Biol. *221*, 295–307.